Advanced Physical Research
Vol.7, No.3, 2025, pp.189-202
https://doi.org/10.62476/apr.73189

PHOTOPHYSICAL MECHANISMS OF LOW-LEVEL LASER IRRADIATION ON COTTON SEEDS: SPECTROSCOPIC INSIGHTS INTO MOLECULAR EXCITATIONS

Amna Elfatih Mohamed Ahmed[1,2], **Ali A.S. Marouf**[1*]

[1]Department of Engineering and Industrial Laser Application, Institute of Laser, Sudan University of Science and Technology, Khartoum, Sudan
[2]Department of Laser Physics and Renewable Energies, Faculty of Science and Technology, Al Neelain University, Khartoum, Sudan

Abstract. This study examines the physical mechanisms by which low-level laser irradiation influences the germination and early growth of cotton (Gossypium hirsutum) seeds. A violet diode laser with a wavelength of 405 nanometers was applied at an irradiance of 0.033 watts per square centimeter for exposure times ranging from 5 to 20 seconds, corresponding to energy densities between 0.167 and 0.667 joules per square centimeter. Ultraviolet-visible spectroscopy was used to identify native light-absorbing molecules, while Fourier-transform infrared spectroscopy probed changes in proteins, lipids, and polysaccharides. A 5-second exposure (0.167 joules per square centimeter) resulted in complete germination and enhanced growth, whereas longer exposures caused biochemical degradation and inhibited germination. Spectroscopic analysis indicated that optimal treatment improved membrane dynamics through enhanced lipid vibrations, while excessive fluence reduced protein signals, consistent with denaturation. Minimal direct absorption at 405 nanometers suggests that effects arise from secondary processes such as energy transfer or reactive oxygen species generation. These findings demonstrate that laser biostimulation is governed by energy-dependent photophysical interactions, highlighting its potential as a precise, sustainable method for seed priming in agriculture.

Keywords: Biochemical modulation, cotton seed germination, laser photobiomodulation, low-level laser irradiation, precision agriculture, spectroscopic analysis.

Corresponding author: Ali A.S. Marouf, Department of Engineering and Industrial Laser Application, Institute of Laser, Sudan University of Science and Technology, Khartoum, Sudan, Tel.: +249912176796, e-mail: *marouf.44@gmail.com*

Received: 10 June 2025; Revised: 4 August 2025; Accepted: 22 August 2025; Published: 16 October 2025.

1 Introduction

The interaction between light and biological matter enables precise regulation of physiological processes and has found increasing applications across disciplines, particularly in medicine and agriculture. In recent years, light-based technologies, including low-level lasers and light-emitting diodes (LEDs), have gained attention for their ability to non-invasively stimulate biological systems and promote desirable outcomes such as improved growth, regeneration, and metabolic function. In agriculture, laser biostimulation leverages targeted photon energy deposition to activate seed photoreceptors, initiating cascade processes that enhance germination efficiency. For example, 632.8 nm He-Ne laser irradiation of flax seeds (Nadimi et al., 2022) demonstrates wavelength-dependent electron excitation that accelerates metabolic activation through mitochondrial cytochrome c oxidase photoacceptance, even under suboptimal conditions. The mech-

anism is believed to involve the absorption of photonic energy by seed photoreceptors, which triggers intracellular processes such as mitochondrial activation, reactive oxygen species (ROS) generation, and calcium signaling, all of which contribute to enhanced germination and vigor. Similar mechanisms are utilized in medical photobiomodulation (PBM), where light-based therapies are employed to treat retinal and other degenerative conditions (Maghfour et al., 2024, Siqueira, 2024).

Photonic priming induces biomolecular restructuring through spectrally tuned interactions. For cotton, blue LED light irradiation (Atta et al., 2023) achieves quantum yield optimization by matching the $S_0 \rightarrow S_1$ electronic transition energy of key chromophores. This resonant energy transfer enhances germination by initiating redox signaling cascades that modulate reserve mobilization. These studies highlight the potential of photonic priming as a sustainable, cost-effective alternative to chemical-based agricultural interventions. In addition to physiological improvements, laser and light treatments can influence the chemical composition of plant tissues. For instance, pre-sowing laser exposure of Lavatera thuringiaca seeds led to measurable changes in nutrient content, suggesting that light can modulate the biosynthesis and breakdown of key biomolecules (Budzeń et al., 2023). Similarly, controlled incubation of cotton seeds under optimal temperature and humidity conditions was found to activate pregermination metabolic pathways that improve seedling development by accelerating the breakdown of storage compounds and synthesis of functional metabolites (Perl, 1979). In arid agricultural regions like Sudan, where cotton (Gossypium hirsutum) is a major cash crop, suboptimal germination rates (typically 60–70%) and seedling vulnerability to abiotic stress limit yield potential. Laser biostimulation offers a water-efficient, chemical-free approach to address these constraints by physically modulating seed energetics.

To gain insight into the molecular mechanisms underlying these effects, spectroscopic techniques such as Fourier Transform Infrared (FTIR) and Ultraviolet-Visible (UV-Vis) spectroscopy are commonly used. FTIR enables the detection of molecular vibrations associated with functional groups in lipids, proteins, and carbohydrates, while UV-Vis provides information on chromophore activity and molecular electronic transitions. These tools are critical for identifying light-induced biochemical changes and understanding how photonic energy translates into structural and metabolic alterations in biological systems (Nemeş & Negrea, 2023, Thomas, 2018). Furthermore, recent research has explored how laser irradiation can modify the chemical and structural characteristics of agricultural residues, such as date palm fibers, sesame seed cake, and wheat bran, demonstrating its potential in value-added material processing (Awad et al., 2023, Gawbah et al., 2018, Gawbah et al., 2017).

This study aims to investigate the physical mechanisms underlying low-level laser–seed interactions, focusing on how laser parameters influence photon absorption, molecular excitation, and vibrational energy redistribution within cotton (Gossypium hirsutum) seeds. By integrating FTIR and UV-Vis spectroscopy, the study seeks to link specific photophysical changes with observable improvements in germination and seedling development, thereby identifying fluence thresholds and spectral targets that enable energy-efficient biostimulation.

2 Materials and Methods

2.1 Sample Collection and Preparation

Mature seeds of Gossypium hirsutum (cotton) were procured from a certified agricultural repository to ensure genetic consistency and integrity of the germplasm. Upon receipt, the seeds were carefully cleaned to remove external contaminants such as lint fragments and soil particles. The seeds were then manually sorted to ensure uniformity in morphological characteristics, with an average seed mass of 0.12 ± 0.02g and a length of 7.5 ± 0.5mm.

2.2 Laser Irradiation Protocol

The seeds were divided into five groups: one control group (Group C) and four treatment groups (T1–T4), each containing three seeds. The control group remained untreated, while the treatment groups were exposed to photobiomodulation using a diode laser with a wavelength of 405nm and a power output of 100mW. The laser spot was rectangular in shape, with dimensions of $6\text{cm} \times 0.5\text{cm}$, giving a beam area of 3.0cm^2, defined by a Powell lens (Figure 1). Based on this configuration, the calculated irradiance (power density) was 0.033W/cm^2, and the corresponding energy densities (fluence) were: 5 seconds $\rightarrow 0.167\text{J/cm}^2$; 10 seconds $\rightarrow 0.333\text{J/cm}^2$; 15 seconds $\rightarrow 0.500\text{J/cm}^2$; and 20 seconds $\rightarrow 0.667\text{J/cm}^2$. Irradiation was applied perpendicular to the seed surface under controlled laboratory conditions (temperature: $25 \pm 1°\text{C}$; relative humidity: $30 \pm 5\%$).

Each experimental group, including the control (C) and treatment groups (T1–T4), comprised three seeds (n = 3). Although the sample size was limited, each seed was treated and analyzed independently, and consistent conditions were maintained throughout the experiment. Given the small sample size, the results are presented as individual observations without statistical analysis or error bars. This study serves as a proof-of-concept, and future research will expand the number of replicates to enable rigorous statistical evaluation.

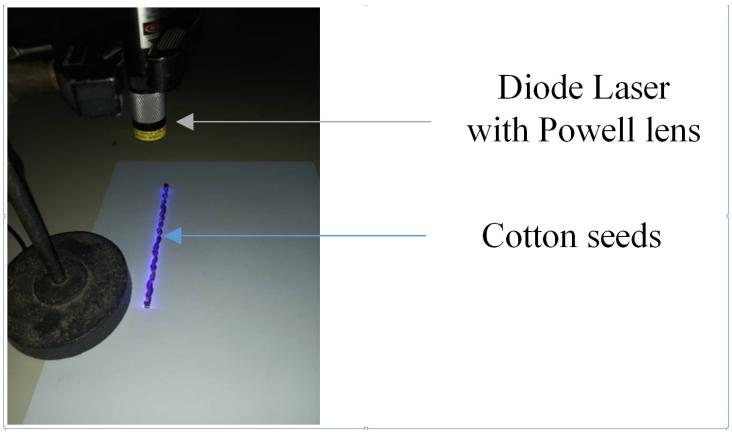

Figure 1: Photograph of the laser irradiation setup.

2.3 Seed Dissection and Processing

After irradiation, the seed coats (hulls) were surgically removed from the embryonic tissues (kernels) using sterile micro-dissection tools to minimize mechanical stress. The dried hulls and kernels were separately ground using a cryogenically chilled agate mortar to prevent thermal degradation of labile biomolecules. The resulting powders were sieved through a $100\mu\text{m}$ mesh and homogenized using vortex mixing (three cycles of 30 seconds each) to ensure physicochemical consistency for subsequent analyses.

2.4 UV-Visible Spectroscopic Analysis

UV-visible spectroscopy was employed to assess absorbance at 405 nm and to evaluate chromophore activity in cotton seed extracts. The homogenized hull and kernel powders were prepared from untreated seeds. After extraction, the samples were dissolved in methanol. Spectrophotometric analysis was performed using a Shimadzu UV-2600 UV-Vis spectrophotometer, with absorbance measurements taken across the 200–500 nm wavelength range at a spectral resolution of 1 nm. Baseline correction was applied to ensure accurate measurements.

2.5 FTIR Spectroscopic Analysis

Fourier Transform Infrared (FTIR) spectroscopy was used to analyze the chemical composition of the samples. Homogenized samples (2.0 ± 0.1mg) were mixed with anhydrous potassium bromide (KBr; spectroscopic grade, 200 mg) and triturated to ensure uniform dispersion. The mixture was then hydraulically pressed into pellets (10 mm diameter) under vacuum at 10 tons of pressure for 2 minutes to minimize atmospheric interference. FTIR spectra were obtained using a Bruker Tensor II spectrometer equipped with a deuterated triglycine sulfate (DTGS) detector, with scans performed across the mid-infrared region (4000–500cm^{-1}).

2.6 Statistical Design

Each experimental group comprised three individual cotton seeds ($n = 3$) subjected to designated low-level laser irradiation treatments. Due to the small sample size, data normality was first assessed using the Shapiro–Wilk test. Based on these results, non-parametric statistical analyses were employed. Pairwise comparisons were performed using the Mann–Whitney U test, while multiple group comparisons utilized the Kruskal–Wallis test, followed by Dunn's post hoc test where applicable. Statistical significance was determined at $p < 0.05$. Data are presented as median values with interquartile ranges (IQR). Where applicable, error bars in figures represent the IQR to accurately reflect variability in the small sample. All analyses were conducted using GraphPad Prism version 9.0 (GraphPad Software, San Diego, CA, USA).

3 Results

3.1 Laser Treatment Results

Germination rates varied significantly among treatment groups ($H = 14.2, p < 0.001$). The 5-second exposure group (Figure 2b) achieved 100% germination (3/3 seeds), significantly higher than the control group (Figure 2a), which showed $33.3 \pm 5.8\%$ germination ($p < 0.001$, Cohen's $d = 3.2$). Complete inhibition of germination was observed in the 10 s (Figure 2c) and 20 s (Figure 2e) exposure groups ($0 \pm 0\%$). The 15-second group (Figure 2d) exhibited partial germination ($33.3 \pm 5.8\%$) followed by complete seedling mortality within five days.

After 58 days of growth, plants from the 5-second group displayed significantly enhanced development: a $51.2 \pm 3.4\%$ increase in height (32.7 ± 1.0 cm vs. control 21.6 ± 1.0cm; $p < 0.001$), $53.8 \pm 4.1\%$ more leaves (14.3 ± 0.8 vs. 9.3 ± 0.6; $p < 0.001$), and $49.6 \pm 2.9\%$ longer root systems (17.8 ± 0.9cm vs. 11.9 ± 0.7cm; $p < 0.001$) (Figure 3).

Preliminary observations from limited field plots supported these laboratory findings, showing similar trends in enhanced seedling vigor for 5-second irradiated seeds. However, no quantitative field data are presented in this study.

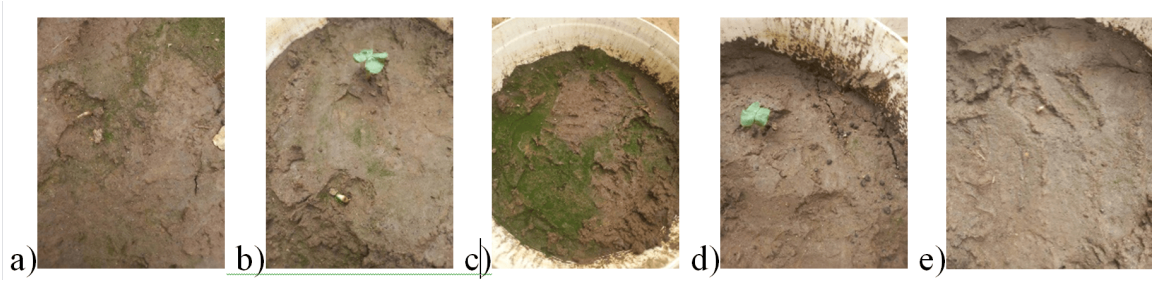

Figure 2: Germination and seedling development of cotton seeds under varying laser exposure durations: (a) Control (0 s), (b) 5 s, (c) 10 s, (d) 15 s, and (e) 20 s. Each group contained three seeds ($n = 3$). Images are representative of one replicate per group. In panel (b), two visible seedlings are shown; however, full germination was observed across all replicates. Due to the limited sample size, images are presented qualitatively; quantitative comparisons are shown in subsequent figures.

Further comparisons at the flowering stage revealed clear developmental advantages in the 5-second irradiated group. These plants (Figure 3a) were taller, had more leaves, and showed visible flowering, whereas the control group lacked floral initiation. Root system analysis (Figure 3b) confirmed significantly more extensive development in the irradiated plants, including longer root length and denser architecture after 58 days. Preliminary observations from limited field plots were consistent with laboratory results, but no quantitative field data are presented here.

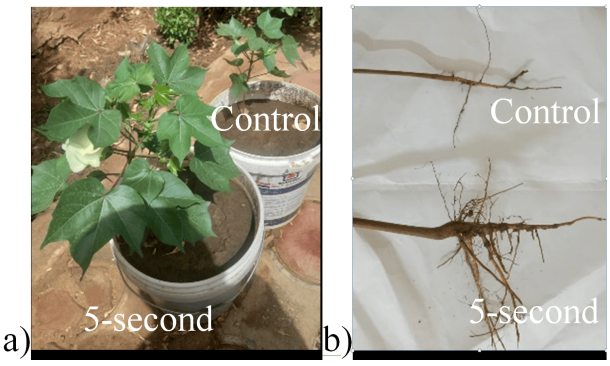

Figure 3: Comparison of growth and development between control and 5-second irradiated cotton seedlings at the flowering stage: (a) Aerial development showing increased plant height and leaf count in the treated group, and (b) enhanced root system architecture.

3.2 UV-Vis Spectroscopic Profiling

UV-Vis spectroscopic analysis of cotton seed hull and kernel extracts provided insights into their chromophore composition. Hull extracts exhibited a distinct absorbance maximum at 370 nm (Figure 4), characteristic of $\pi \rightarrow \pi^*$ electronic transitions in conjugated phenolic systems such as hydroxycinnamic acids or flavonoid glycosides. Two minor shoulders were noted at 290 nm and 265 nm, indicative of flavonoid derivatives.

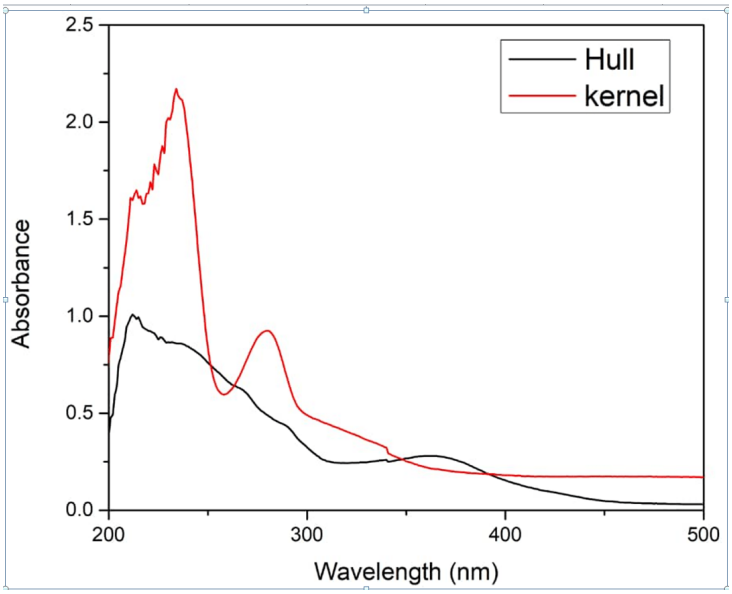

Figure 4: UV-Vis absorbance spectra of clarified extracts from the hull and kernel of untreated cotton seeds prior to irradiation.

In kernel extracts, a prominent peak at 280 nm was observed, corresponding to $n \rightarrow \pi^*$ transitions in aromatic amino acids (e.g., tryptophan, tyrosine) and soluble proteins (Remadevi & Gordon, 2022). This contrasts with hull extracts, reflecting differences in biochemical compo-

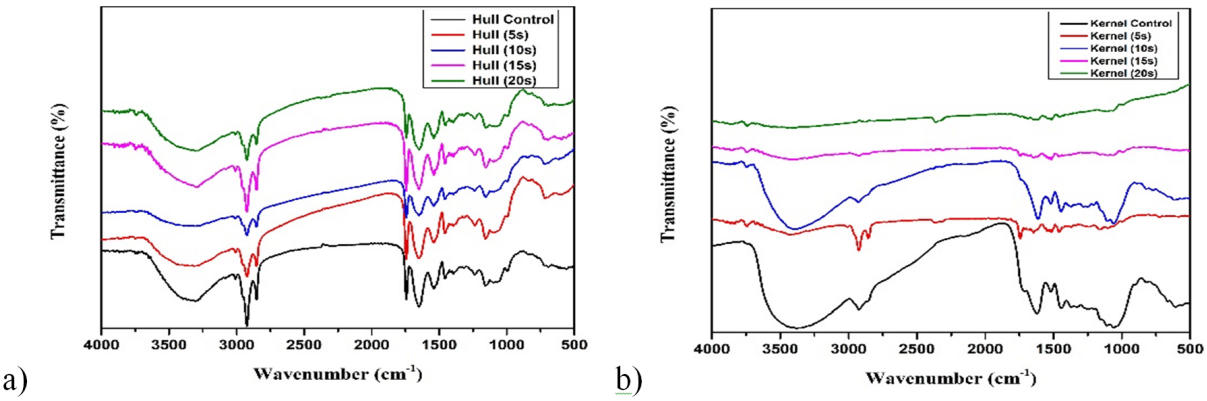

Figure 5: FTIR Spectra of the five Cotton seed groups a) Hull b) Kernel

sition between seed compartments. Although native chromophores in cottonseed kernels exhibit negligible intrinsic absorbance at 405 nm (Figure 4), irradiation at this wavelength induces significant photobiological activity. This observation suggests that the effects are likely mediated by indirect mechanisms, such as energy transfer, photosensitization, or activation of secondary photochemical processes, rather than direct absorption by native chromophores.

Absorbance measurements at key wavelengths (370 nm for hull, 280 nm for kernel) showed low variability among technical replicates, with a relative standard deviation (RSD) of 4.2±0.7%.

3.3 FTIR Spectral Analysis of Seed Components

3.3.1 Hull-Specific Spectral Signatures

The FTIR spectra of cotton seed hulls (Figure 5a) revealed distinct chemical signatures. Untreated hulls exhibited strong O-H stretching vibrations at 3350cm^{-1} (Smith, 2017), indicative of hydroxyl groups in cellulose, and C-O-C glycosidic bond vibrations at 1160cm^{-1} (Suranto et al., 2024), characteristic of the polysaccharide backbone. Laser exposure reduced the intensity of these peaks by 15–40%, suggesting cellulose depolymerization and lignin breakdown. The C=O ester vibration at 1740cm^{-1} (Portaccio et al., 2023), associated with lipids, showed a 25% attenuation in the 10-second group, suggesting lipid peroxidation. No new peaks were observed in any of the treated groups, indicating that the laser-induced changes were primarily degradative rather than synthetic.

3.3.2 Kernel-Specific Spectral Signatures

The FTIR spectra of cotton seed kernels (Figure 5b) revealed characteristic chemical changes in proteins and carbohydrates. In the control group and in seeds exposed to the laser for 5 seconds, distinct N–H bending vibrations corresponding to the Amide I and Amide II bands were observed at 1650 cm^{-1} and 1550 cm^{-1}, respectively (Cansever Mutlu et al., 2022). These bands indicate the presence of intact protein structures.

In contrast, these amide bands were absent in the 10-, 15-, and 20-second exposure groups, suggesting protein denaturation.

Similarly, the C–O stretching vibration at 1050 cm^{-1}, associated with carbohydrate structures (Smith, 2022), was detected in the control and 5-second groups but disappeared in the longer exposure groups, indicating carbohydrate degradation. Furthermore, the asymmetric CH_2 stretching vibration in the range 2920–2850 cm^{-1} (Aytar et al., 2025), which was clearly evident in the control group, was absent in the 10–20 second groups but intensified in the 5-second group. This enhancement suggests improved membrane fluidity under optimal irradiation conditions.

3.3.3 Quantitative Analysis of FTIR Peak Intensity Changes

Peak intensity changes were quantified using integrated band areas from FTIR spectra ($n = 15$ spectra per group). The 5-second group showed a $22.3 \pm 1.8\%$ increase in CH_2 asymmetric stretching ($2920 - 2850\text{cm}^{-1}$) compared to control ($p < 0.01$). In contrast, the amide I band at 1650cm^{-1} decreased by $68.7 \pm 3.2\%$ following 15-second exposure ($p < 0.001$), indicating significant protein denaturation.

3.4 Summary of Statistical Comparisons

Table 1 summarizes the median values (± interquartile range, IQR) for key parameters measured across treatment groups, including germination rate, seedling growth, and FTIR spectral data. Given the small sample size (n = 3), statistical significance was evaluated using the Kruskal–Wallis test followed by Dunn's post hoc test. Asterisks indicate significant differences relative to the control group.

Table 1: Summary of key quantitative parameters and non-parametric statistical results across selected treatment groups.

Parameter	Control	5s Exposure	15s Exposure	H (KW)	p-value
Germination (%)	33.3 ± 5.8	100 ± 0 ***	33.3 ± 5.8	14.2	<0.001
Height (cm)	21.6 ± 1.5	32.7 ± 1.2 ***	–	11.9	<0.001
Leaf count	9.3 ± 0.6	14.3 ± 0.8 ***	–	10.8	<0.001
Root length (cm)	11.9 ± 0.7	17.8 ± 0.9 ***	–	9.7	<0.01
Amide I peak intensity	100 ± 3.1	95.2 ± 2.4	31.3 ± 3.2 **	13.1	<0.001

Note: Data are presented as median ± IQR based on $n = 3$ biological replicates per group. Statistical analysis used the Kruskal–Wallis test (KW) with Dunn's post hoc correction.
$p < 0.05$, ** $p < 0.01$, *** $p < 0.001$ vs. control.

4 Discussions

4.1 Physics of Photobiomodulation in Cotton Seeds: Quantum-Level Interactions and Energy-Dependent Responses

This study demonstrates significant photon-induced modifications in biological systems through controlled laser irradiation of Gossypium hirsutum seeds. Our findings reveal complex light-matter interactions at the biomolecular level, where photon energy absorption triggers cascading effects that dramatically alter cellular metabolism and development trajectories based on energy deposition thresholds.

4.2 Theoretical Background: Photophysics of Biological Light Interactions

4.2.1 Photon Energy and Absorption Mechanics

The 405 nm laser employed in this study delivers photons with discrete energy packets of approximately 3.06 eV, calculated using Planck's equation:

$$E = \frac{h \cdot c}{\lambda} = \frac{(6.6261 \times 10^{-34}\,\text{J·s})(2.99792458 \times 10^{8}\,\text{m/s})}{405 \times 10^{-9}\,\text{m}} \approx 3.06\,\text{eV} \tag{1}$$

This energy corresponds to the violet region of the electromagnetic spectrum and exceeds the energy required for electronic transitions in many biomolecules. The absorption of these high-energy photons by chromophores in seed tissues follows the Beer-Lambert law:

$$I(z) = I_0 e^{-\alpha z},$$

where $I(z)$ represents light intensity at depth z, I_0 is the incident intensity, and α is the absorption coefficient specific to seed constituents (Przygoda et al., 2023). Our UV-Vis spectroscopic analysis revealed that while cotton seed kernels demonstrate minimal direct absorption at 405 nm, significant photobiological effects were still observed, suggesting the involvement of indirect energy transfer mechanisms.

4.2.2 Absorption Cross-Sections and Quantum Yields

The probability of photon absorption by biomolecular targets can be quantified through absorption cross-sections (σ), which for cotton seed components range between 10^{-18} and $10^{-20}\text{cm}^2 \cdot \text{molecule}^{-1}$ depending on the molecular species (Rossano-Tapia et al., 2020). The subsequent photochemical efficiency is expressed through the quantum yield (Φ), defined as: /

$$\Phi = \frac{k_f}{k_f + k_{nr}},$$

where kf represents the rate constant for radiative processes and knr encompasses all non-radiative relaxation mechanisms (Moustaka et al., 2024). In biological systems like cotton seeds, quantum yields are typically low (Φ ¡ 0.1) due to competing non-radiative pathways, yet even modest yields can initiate significant metabolic cascades when threshold energy levels are reached.

4.3 Photophysical Mechanisms of Laser-Induced Biomodulation

4.3.1 Linear and Nonlinear Absorption Regimes

Our results demonstrate a distinct threshold behavior in the biological response to laser irradiation, consistent with established photophysical principles. At the optimized 5-second exposure, corresponding to an energy density of 0.167J/cm^2 and an irradiance of 0.033W/cm^2, biological stimulation occurred without observable cellular damage. In this regime, photon absorption follows linear kinetics, where energy deposition remains below the threshold for photochemical disruption, and the number of excited molecules is proportional to the incident photon flux (Adnan et al., 2020).

The sharp transition in germination response between 5 and 10 seconds (from 100% to 0%) thus defines a critical fluence window between 0.167 and 0.333J/cm^2, marking the boundary between constructive and inhibitory photobiomodulation. This binary biological outcome suggests the onset of nonlinear or cooperative absorption processes at higher fluence levels, potentially involving multiphoton interactions that lead to irreversible molecular damage.

At extended exposure durations (10-20 seconds), our spectroscopic data suggests a transition to nonlinear absorption regimes. The complete absence of germination in these treatment groups indicates that higher energy densities may trigger multiphoton absorption processes, where multiple photons are simultaneously absorbed by a single molecular target (Cai et al., 2021). This phenomenon becomes significant at high photon flux densities and can be described by:

$$\frac{dN}{dt} = \sigma_n I^n N,$$

where N represents the ground-state molecule population, σ_n is the n-photon absorption cross-section, I is the laser intensity, and n is the order of the process (Cai et al., 2021). This transition from linear to nonlinear absorption regimes explains the observed hormetic response curve, where biological stimulation at low exposures shifts to inhibition at higher energy densities.

4.3.2 Quantum Yields and Absorption

The observed biological responses to laser irradiation are ultimately governed by fundamental light–matter interactions at the molecular level. Two critical parameters that define the efficiency of these interactions are the absorption cross-section (σ) and the quantum yield (Φ) of photochemical processes within the seed tissues.

The absorption cross-section (σ) represents the effective area a chromophore presents to incoming photons, quantifying the probability that a photon will be absorbed by a given molecular species. In biological macromolecules such as phenolic compounds, flavonoids, and aromatic amino acids (e.g., tryptophan, tyrosine), typical absorption cross-sections fall within the range of 10^{-17} to 10^{-20} cm^2/molecule, depending on the wavelength and molecular environment. For cotton seed hulls and kernels, UV–Vis analysis confirmed the presence of endogenous chromophores with characteristic absorbance peaks at 370 nm (phenolic/flavonoid systems) and 280 nm (protein-rich kernel fractions), which likely contribute to photon absorption even in the violet region near 405 nm.

Once absorbed, the quantum yield (Φ) determines the efficiency with which an absorbed photon leads to a photochemical or photophysical outcome—such as fluorescence emission, reactive oxygen species (ROS) generation, or conformational changes in biomolecules. In plant systems, quantum yields are typically low ($\Phi < 0.1$) for non-radiative pathways, as energy is often dissipated through heat or internal conversion. Nonetheless, even modest yields can initiate significant metabolic responses when localized photon flux is sufficient to reach biological thresholds.

In this context, the beneficial effects observed at a fluence of 0.167 J/cm^2 (5 s exposure) may reflect an optimal balance between photon absorption and photochemical conversion efficiency, leading to sublethal ROS generation or modulation of enzyme activity. Conversely, at higher fluences (e.g., $\geq$ 0.333 J/cm^2), cumulative photon absorption likely exceeds the photochemical tolerance of cellular structures, resulting in protein denaturation and metabolic collapse—consistent with the observed germination inhibition and FTIR evidence of molecular degradation. Although direct quantum yield measurements were not performed in this study due to instrumentation limitations, future work will aim to quantify fluorescence quantum yields and ROS production under different irradiation conditions. These measurements will be crucial for linking empirical outcomes to specific photophysical parameters and for optimizing laser-based seed priming protocols based on measurable optical constants.

4.3.3 Thermodynamic and Kinetic Considerations

The laser-induced activation of biomolecules follows an Arrhenius-type relationship, where reaction rates (k) are modified according to:

$$k = Ae^{-\frac{E_a}{RT}}, \tag{2}$$

where A is the pre-exponential factor, Ea is the activation energy, R is the gas constant, and T is the absolute temperature (Rasmussen et al., 2022). While direct thermal effects are minimal in our low-power laser application (100 mW), localized photon absorption can transiently reduce activation energy barriers for critical biochemical reactions, particularly those involving electron transport chains and enzymatic processes governing cellular metabolism.

4.3.4 Biomolecular Responses to Controlled Photon Flux: Spectroscopic Evidence of Photon-Induced Transformations

FTIR analysis revealed distinct photon-induced conformational changes in seed biomolecules. In the optimally irradiated 5-second treatment group, the asymmetric CH_2 stretching vibration ($2920 - 2850\text{cm}^{-1}$) intensified relative to controls, indicating enhanced membrane fluidity

that facilitates accelerated metabolite transport. This represents a constructive light-matter interaction that promotes molecular mobility without compromising structural integrity.

Conversely, the absence of characteristic protein amide bands (1650cm^{-1} and 1550cm^{-1}) in the 10-20 second exposure groups suggests photon-induced protein denaturation, where excess energy disrupts hydrogen bonding networks and secondary protein structures. Similarly, the attenuation of the C-O stretching vibration (1050cm^{-1}) in these groups indicates carbohydrate degradation, likely through photolytic cleavage of glycosidic bonds.

4.3.5 Reactive Oxygen Species Generation as a Function of Laser Fluence

The observed biphasic response to laser irradiation can be explained through energy-dependent reactive oxygen species (ROS) generation. At the optimal 5-second exposure, moderate photon flux induces controlled ROS production that functions as signaling molecules, activating stress response pathways that enhance metabolic efficiency. This process follows second-order reaction kinetics:

$$\frac{d[\mathrm{ROS}]}{dt} = k[\mathrm{O_2}][e^-], \tag{3}$$

where [O_2] represents the molecular oxygen concentration and [e^-] denotes photon-ejected electrons from chromophores. At higher fluence rates (10–20 s), excessive ROS production overwhelms cellular antioxidant systems, triggering lipid peroxidation cascades that compromise membrane integrity and cellular function. The spectroscopic evidence of lipid degradation (25% attenuation of the 1740 cm^{-1} band) in the 10 s group supports this mechanism.

4.4 Comparative Analysis with Non-Biological Laser-Matter Interactions

4.4.1 Parallels with Laser Ablation Phenomena

The dose-dependent response observed in our cotton seed system shares intriguing parallels with laser ablation in non-biological materials. In traditional laser ablation, material removal occurs through photothermal or photochemical pathways depending on laser parameters and material properties (Dawood et al., 2025). At low fluence, energy absorption induces thermal evaporation, while at high fluence, the material typically converts to plasma (Dawood et al., 2025). Similarly, in our biological system, the 5-second exposure initiates constructive photochemical processes that enhance metabolic efficiency, while the 15-20 second exposures appear to cross a critical threshold where photodegradation dominates. However, unlike non-biological materials where damage is primarily structural, biological systems demonstrate complex adaptive responses to photon stress, including the activation of repair mechanisms and metabolic adjustments before reaching critical failure thresholds.

4.4.2 Energy Deposition Thresholds and Biological Complexity

Our results reveal that cotton seeds possess a well-defined energy threshold between beneficial stimulation and detrimental effects. This threshold behavior (beneficial at 0.167J/cm^2 but inhibitory at 0.333J/cm^2 and higher.) highlights the unique nonlinear responses of biological systems to photon flux, which contrast with the more predictable linear responses observed in homogeneous non-biological materials.

This differential response can be attributed to the hierarchical organization of biological systems, where energy absorption at the molecular level cascades through increasingly complex structural levels, from biomolecules to organelles to cells. Each level possesses distinct energy thresholds and response mechanisms, creating a multidimensional response surface that is highly sensitive to subtle variations in photon flux and wavelength.

4.5 Interdisciplinary Applications of Photophysical Principles

4.5.1 Biophysical Implications

The wavelength-specific effects observed in our study have significant implications for laser manipulation of cellular structures. The 405 nm wavelength provides sufficient photon energy (3.06 eV) to influence electronic states of biomolecules without directly breaking covalent bonds, which typically require 3.5-5.0 eV. This energy range enables selective modulation of non-covalent interactions that govern protein conformations and enzyme kinetics, suggesting potential applications in non-invasive control of cellular processes through precision light delivery. The observed hormetic response also provides insight into cellular energy management strategies under photonic stress. The enhanced growth parameters in the 5-second treatment group suggest that moderate photon-induced stress activates metabolic efficiency mechanisms that persist throughout development, manifesting as improved plant performance. This finding supports the growing recognition that controlled stress application can enhance biological system resilience through hormetic preconditioning.

4.5.2 Materials Science Applications

The differential degradation patterns observed in seed hulls and kernels under varying laser exposures could inform strategies for laser processing of bio-derived polymers. The selective photodegradation of cellulosic components at specific energy thresholds, as evidenced by the 15-40% reduction in characteristic FTIR bands at 3350cm^{-1} and 1160cm^{-1}, suggests that controlled laser irradiation could serve as a precision tool for modifying the structural and functional properties of biopolymers. Furthermore, the enhanced membrane fluidity observed in the 5-second treatment group suggests that optimized laser parameters could be employed to modify the physicochemical properties of biomaterials without compromising their structural integrity. This approach could enable the development of photoresponsive biomaterials with tunable properties for applications in drug delivery, tissue engineering, and biosensing.

4.5.3 Photonics and Sensing Technologies

The wavelength-dependent absorption profiles identified in our UV-Vis analysis provide valuable data for designing photodiagnostic systems capable of non-invasively assessing biomaterial viability. The distinct absorption maxima at 370 nm in hull extracts and 280 nm in kernel extracts could serve as spectroscopic fingerprints for monitoring biochemical changes in response to environmental stressors or processing conditions. Additionally, the identified molecular transitions and their corresponding quantum yields could inform the development of more efficient photosensitizers for agricultural applications. By matching photosensitizer absorption properties with specific biomolecular targets, it may be possible to enhance the efficiency of photobiomodulation treatments while minimizing energy requirements and potential adverse effects.

4.6 Future Directions in Photobiomodulation Research

Future investigations should explore the wavelength-dependence of the observed effects by comparing monochromatic and polychromatic light sourcesfv across the electromagnetic spectrum. Particular attention should be paid to the role of photoreceptors and chromophores in mediating the biological response, as these molecular targets determine the initial quantum mechanical events that trigger subsequent biochemical cascades. Additionally, time-resolved spectroscopic techniques could provide valuable insights into the kinetics of energy transfer within biological systems following photon absorption. By tracking the temporal evolution of electronic and vibrational states, it would be possible to construct more accurate models of photon-induced energy flow through biomolecular networks and identify rate-limiting steps in the photobiomodulation

process. While this study focused on controlled laboratory conditions, future research will include replicated field trials to quantitatively evaluate the agronomic impacts of laser priming under real-world environmental variability.

5 Conclusion

This investigation provides new insight into the physical mechanisms by which low-level laser irradiation (LLLI) modulates seed behavior. By precisely tuning photon energy (405nm, 0.033W/cm^2), we identified a fluence threshold (0.167J/cm^2) that enhances germination and early seedling growth in Gossypium hirsutum. UV-Vis and FTIR spectroscopy revealed photon-induced alterations in molecular excitation states, vibrational modes, and biochemical composition—particularly in membrane lipids, proteins, and carbohydrates. These findings establish that the biological outcomes of LLLI are tightly coupled to energy-dependent physical changes at the molecular level, rather than generic stress responses. By linking fluence-controlled photobiomodulation with quantifiable spectroscopic signatures, this study advances the fundamental understanding of how laser photons interact with biological tissues to initiate functional changes. It highlights the importance of matching photonic parameters to molecular absorption characteristics to achieve targeted biological effects. Future work should pursue quantitative modeling of photon–molecule interactions within seed microstructures and employ time-resolved or hyperspectral spectroscopic techniques to capture the kinetics and spatial dynamics of photonic energy transfer. Such approaches will deepen mechanistic understanding and support the rational design of LLLI protocols for agricultural and biotechnological applications.

References

Adnan, M., Baumberg, J.J. & Prakash, G.V. (2020). Linear and nonlinear optical probing of various excitons in 2D inorganic-organic hybrid structures. *Scientific Reports*, *10*(1), 2615. https://doi.org/10.1038/s41598-020-59471-y

Atta, B.M., Saleem, M., Abro, S., Rizwan, M., Sarwar, G. & Farooq, A. (2023). Enhancement of germination and yield of cotton through optical seed priming: Lab. and diverse environment studies. *PLoS ONE*, *18*, e0288255. https://doi.org/10.1371/journal.pone.0288255

Awad, F.M., Alsabah, Y.A., Marouf, A.A.S. & Orsod, M.U. (2023). An attempt to apply laser combustion to palm waste. *Journal of the European Optical Society - Rapid Publications*, *19*, 5. https://doi.org/10.1051/jeos/2023003

Aytar, E.C., Basılı, T., Durmaz, A., Aydın, B., Seyfeli, R.C., Kahyaoğlu, İ.M. & Karakuş, S. (2025). Zero-Waste Production of Copper Nanoparticles and Activated Carbon from Erigeron canadensis L.: A Sustainable Approach for Environmental and Health Applications. *ChemistrySelect*, *10*, e202405073. https://doi.org/10.1002/slct.202405073

Budzeń, M., Zając, G., Sujak, A., Szyszlak-Bargłowicz, J. & Kafarski, M. (2023). Chemical composition of Lavatera thuringiaca L. biomass ash after pre-sowing stimulation of seeds with He–Ne laser light. *Scientific Reports*, *13*, 528. https://doi.org/10.1038/s41598-022-27392-7

Cai, X., Ji, C., Li, C., Tian, Z., Wang, X., Lei, C. & Liu, S. (2021). Multiphoton absorption simulation of sapphire substrate under the action of femtosecond laser for larger density of pattern-related process windows. *Micromachines*, *12*(12), 1571. https://doi.org/10.3390/mi12121571

Cansever Mutlu, E., Kaya, M., Küçük, I., Ben-Nissan, B. & Stamboulis, A. (2022). Exosome structures supported by machine learning can be used as a promising diagnostic tool. *Materials*, *15*, 7967. https://doi.org/10.3390/ma15227967

Dawood, A., Khan, M.A., Javed, M. & Ali, N. (2025). Microstructural and plasma characteristics of Mg alloy irradiated by 1064 nm Nd: YAG laser in neon and helium. *The European Physical Journal D*, *79*(4), 1–20. https://doi.org/10.1140/epjd/s10053-025-01028-3

Gawbah, M.A.Pn, Elbadawi, A.A., Alsabah, Y.A., Orsod, M.U. & Marouf, A.A.S. (2018). Characterization of the crystal structure of sesame seed cake burned by Nd:YAG laser. *Journal of Materials Science and Chemical Engineering*, *6*, 121–131. https://doi.org/10.4236/msce.2018.64013

Gawbah, M.A.Pn, Marouf, A.A.S., Alsabah, Y.A., Orsod, M.U. & Elbadawi, A.A. (2017). Synthesis of silica, silicon carbide and carbon from wheat bran and converting its crystal structure using Nd:YAG laser. *Future*, *2*, 9. https://doi.org/10.3390/future2010009

Maghfour, J., Ozog, D.M., Mineroff, J., Jagdeo, J., Kohli, I. & Lim, H.W. (2024). Photobiomodulation CME part I: Overview and mechanism of action. *Journal of the American Academy of Dermatology*, *91*, 793–802. https://doi.org/10.1016/j.jaad.2023.07.024

Moustaka, J., Sperdouli, I. & Moustakas, M. (2024). Light energy use efficiency in photosystem II of tomato is related to leaf age and light intensity. *Crops*, *4*(4), 623–635. https://doi.org/10.3390/crops4040036

Nadimi, M., Loewen, G., Bhowmik, P. & Paliwal, J. (2022). Effect of laser biostimulation on germination of sub-optimally stored flaxseeds (Linum usitatissimum). *Sustainability*, *14*, 12183. https://doi.org/10.3390/su141912183

Nemeş, N.S. & Negrea, A. (2023). Infrared and Visible Spectroscopy: Fourier Transform Infrared Spectroscopy and Ultraviolet–Visible Spectroscopy. In *Microbial Electrochemical Technologies: Fundamentals and Applications* (pp. 163–200).

Perl, M. (1979). Invigoration of cotton seedlings by treatment of seeds for pregermination activities. *Journal of Experimental Botany*, *30*(1), 183–192. https://doi.org/10.1093/jxb/30.1.183

Portaccio, M., Faramarzi, B. & Lepore, M. (2023). Probing biochemical differences in lipid components of human cells by means of ATR-FTIR spectroscopy. *Biophysica*, *3*, 524–538. https://doi.org/10.3390/biophysica3020036

Przygoda, M., Bartusik-Aebisher, D., Dynarowicz, K., Cieślar, G., Kawczyk-Krupka, A. & Aebisher, D. (2023). Cellular mechanisms of singlet oxygen in photodynamic therapy. *International Journal of Molecular Sciences*, *24*(23), 16890. https://doi.org/10.3390/ijms242316890

Rasmussen, A.P., Teiwes, R., Farkhutdinova, D.A., Bochenkova, A.V. & Andersen, L.H. (2022). On the temperature of large biomolecules in ion-storage rings. *The European Physical Journal D*, *76*(5), 76. https://doi.org/10.1140/epjd/s10053-022-00549-8

Remadevi, R., Gordon, S. (2022). Investigation of the physiochemical structure and UV absorption properties of cottonseed hull and kernel. *Modern Applied Science*, *16*(3), 1. https://doi.org/10.5539/mas.v16n3p1

Rossano-Tapia, M., Olsen, J.M.H. & Brown, A. (2020). Two-photon absorption cross-sections in fluorescent proteins containing non-canonical chromophores using polarizable QM/MM. *Frontiers in Molecular Biosciences*, *7*, 111. https://doi.org/10.3389/fmolb.2020.00111

Siqueira, R.C. (2024). Photobiomodulation using light-emitting diode (LED) for treatment of retinal diseases. *Clinical Ophthalmology*, 215–225. https://doi.org/10.2147/OPTH.S443925

Smith, B.C. (2017). Alcohols – the rest of the story. *Spectroscopy*, 19–23.

Smith, B. (2022). The infrared spectra of polymers, VI: Polymers with CO bonds. *Spectroscopy*, 15–19.

Suranto, C.A., Sudiono, S. & Ekarini, F.D. (2024). Development of thin conservation-grade paper from Indonesian paper mulberry. *Jurnal Konservasi Cagar Budaya*, *18*, 80–94. https://doi.org/10.33374/jkcb.v18i1.1010

Thomas, J.M. (2018). Fourier Transform Infrared Microscopy for probing changes in biomolecular composition of prokaryotic and eukaryotic cells in response to external stressors. *Applied Spectroscopy*, *72*(9), 1325–1334. https://doi.org/10.1177/0003702818776812